

**AUTOMATED DETECTION OF MARTIAN DUST DEVIL TRACKS.** T. Statella<sup>1</sup>, P. Pina<sup>2</sup> and E. A. Silva<sup>3</sup>

<sup>1</sup>Instituto Federal de Educação, Ciência e Tecnologia de Mato Grosso, rua Zulmira Canavarros n° 95, Cuiabá, Brasil, e-mail: [thiago.statella@cba.ifmt.edu.br](mailto:thiago.statella@cba.ifmt.edu.br), <sup>2</sup>CERENA, Instituto Superior Técnico, Av. Rovisco Pais, Lisboa, Portugal, e-mail: [ppina@ist.utl.pt](mailto:ppina@ist.utl.pt), <sup>3</sup>Universidade Estadual de São Paulo, rua Roberto Simonsen n° 305, Presidente Prudente, Brasil, e-mail: [erivaldo@fct.unesp.br](mailto:erivaldo@fct.unesp.br).

**Introduction:** Many researchers have been studying dust devils in an attempt to better understand the phenomena. Generally, the research fields comprise mechanic and numerical simulation of dust devils in laboratories, methodologies for recognition of dust devils plumes from rovers on Mars surface, detection of plumes and tracks from orbital images. Despite the number of papers regarding the subject, none of them addresses the automatic detection of dust devils tracks which is an important issue as the amount of images taken grows at a rate greater than the human capability to analyze them. As examples of the difficulty in analyzing manually so many images, several authors [1, 2, 3, 4, 5] had to search for tracks in (3,000), (8,116), (1,238), (1,700) and (6,002) MOC images, respectively. This abstract briefly describes a novel method to detect Martian dust devil tracks automatically. Initially, a total of 124 images (75 MOC narrow angle panchromatic band and 49 HiRISE red band) showing dark dust devil tracks were considered as dataset. The albedo of the tracks varies significantly from scene to scene as does the morphology and landform. In order to decrease the time of processing (mainly because of the size of HiRISE images) and discard irrelevant information (like areas with no tracks) the images were cut to its regions of interest, making a set of 200 images (90 MOC and 110 HiRISE), distributed over the regions of Aeolis, Noachis, Argyre, Eridania and Hellas. Figure 1 shows the location of the set of images according to their coordinates in the planetocentric system. Yellow and red circles locate, respectively, HiRISE and MOC images on surface of Mars.

**Method:** The method starts with an initial filtering by morphological surface area closing and opening, which is equivalent to the union of all openings  $\gamma$  with the connected Structuring Elements (SE)  $B$  whose size in number of pixels equals  $\lambda$ , that is

$$\gamma_\lambda = \vee_i \{ \gamma_{B_i} \mid B_i \text{ with } Area(B_i) = \lambda \} \quad (1)$$

where  $\vee$  is the supremum operator.

The definition of surface area closing is obtained by duality from area opening. Next, a morphological path closing is applied. They can be defined by duality from the definition of path openings given as follows. Let  $E$  be the image domain endowed with a binary adjacency relation  $x \rightarrow y$ . We call  $x$  a predecessor of  $y$

and  $y$  a successor of  $x$ . Using the adjacency relation it is possible to define a dilation by writing

$$\delta(\{x\}) = \{y \in E \mid x \rightarrow y\}. \quad (2)$$

The  $L$ -tuple  $\mathbf{a} = (a_1, a_2, \dots, a_L)$  is called a  $\delta$ -path of length  $L$  if  $a_k \rightarrow a_{k+1}$ . The set of all  $\delta$ -paths of length  $L$  contained in a subset  $X$  of  $E$  is denoted by  $\Pi_L(X)$ . Then the path opening  $\gamma_L$  is the union of all paths of length  $L$  contained in  $X$ , and we can write

$$\gamma_L(X) = \bigcup \{ \mathbf{a} \mid \mathbf{a} \in \Pi_L(X) \}. \quad (3)$$

This equation can be extended to gray level images by the principle of threshold decomposition. The search for the paths is done in four directions ( $0^\circ$ ,  $45^\circ$ ,  $90^\circ$  and  $135^\circ$ ) of the grid according to the rules defined by [6]. The lengths of the paths are defined by the diagonal length of the images times two (although the path closings being used are the constrained ones defined by [6], they still may zig-zag a little so the biggest possible path in the worse case would be the image diagonal times two). Next, the resulting images are binarized by Otsu method to detect the tracks.

**Results and Discussion:** This method was applied to the 200 images of the dataset.

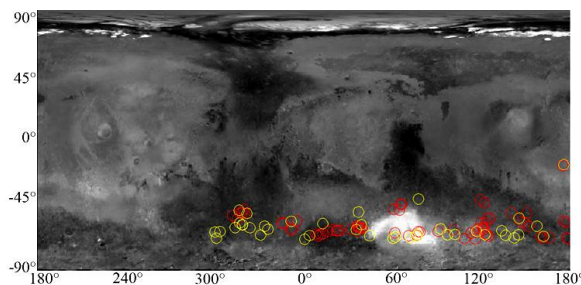


Fig. 1 – Distribution of the images on surface of Mars (yellow circles: HIRASE; red circles: MOC). Image credits: NASA/JPL/MSSS.

The results for the images PSP\_002548\_1255 and E13-00271 (Figs. 2(a) and 3(a)) are shown in Figs. 2(b) and 3(b). The analysis of the results is based on the following measurement:

$$Accuracy = (TP + TN) / (m \times n) \quad (4)$$

where  $TP$  stands for *true positives*,  $TN$  for *true negatives* and  $m \times n$  is the image dimension.  $TP$  and  $TN$  are defined relative to a ground truth or reference image. For a processed image  $PI$  and a ground truth image  $GT$ ,  $TP$  and  $TN$  are calculated as

$$TP = \text{Area}(GT \cap PI), TN = \text{Area}(\sim GT \cap \sim PI) \quad (5)$$

where  $\cap$  and  $\sim$  are the operators *intersection* and *negation*, respectively. For each of the 200 images processed, a ground truth image was made manually by an expert on a computer screen. As examples, the ground truth made for image PSP\_002548\_1255 is shown in Fig. 2(c) and the one made for image E13-00271 is shown in Fig. 3(c). For the image PSP\_002548\_1255 the accuracy was 94.14%, and for image E13-00271 it was 96.12%.

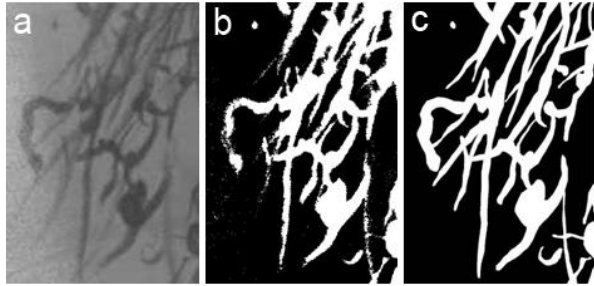


Fig. 2 – Image PSP\_002548\_1255: (a) original, (b) detection and (c) ground truth.

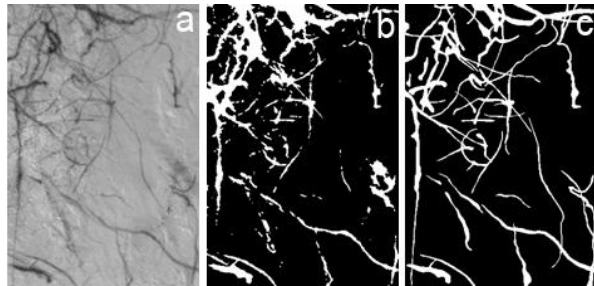


Fig. 3 – Image E13-00271: (a) original, (b) detection and (c) ground truth.

Table 1 summarizes statistics of the analysis for the whole set of images. The solar longitude ( $L_s$ ) of the images varied between  $11.22^\circ$  and  $353.90^\circ$  (basically comprising Martian spring and summer). The local time varied between 13:22h and 16:00h. The spatial resolution of HiRISE images were either 0.25m (~90% of the images) or 0.50m and the spatial resolution of the MOC images varied between 1.43m and 8.75m with mean value of  $4.70\text{m} \pm 1.44\text{m}$ .

Table 1 - Summary of the quality analysis.

	Width (pixels)	Length (pixels)	Accuracy (%)
<b>Min.</b>	138.00	179.00	69.15
<b>Average</b>	2,754.85	2,457.47	92.02
<b>Std</b>	2,445.29	1,845.91	4.87
<b>Max.</b>	9,058.00	7,526.00	99.34

It is also important to notice that the accuracy was not affected by the variation in spatial resolution of the images. The method works for MOC NA as much as for HiRISE. Besides, the method is not sensitive to variations in latitude and solar longitude. This is easy to tell by noticing that no groups were formed when plotting accuracy versus latitude (Fig. 4) and versus solar longitude (Fig. 5) for MOC NA and HiRISE images.

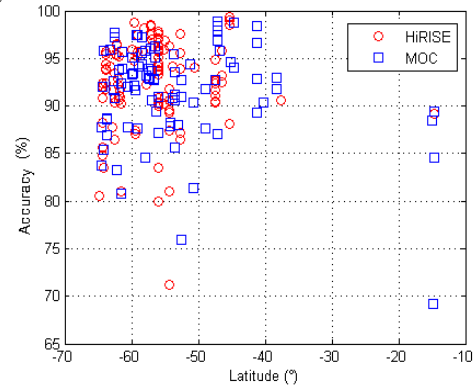


Fig. 4 – Accuracy versus latitude: there is no clustering so the method is latitude independent.

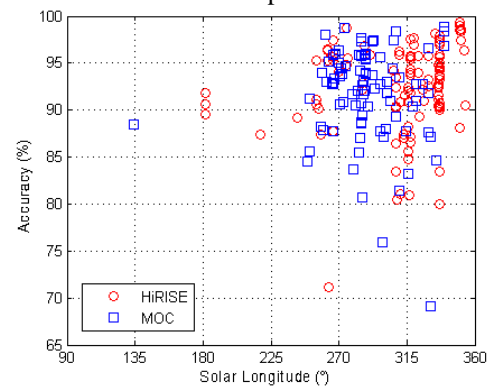


Fig. 5 – Accuracy versus  $L_s$ : the results do not show any dependence to the variation in solar longitude.

**Conclusion:** This paper presented a method for detecting Martian dust devils tracks automatically which achieved  $92.02\% \pm 4.87\%$  of accuracy for 200 MOC NA and HiRISE images. It succeeds in detecting tracks despite the variation in size and spatial resolution of the images, and works for a great range of albedo variation.

**References:** [1] Balme M.R. et al. (2003) *JGR*, 108, E8. [2] Fisher J. A. et al. (2005) *JGR*, 110. [3] Cantor B. A. et al. (2006) *JGR*, 111, 1-49. [4] Örmö J. and Komatsu G. (2003), *JGR*, 108. [5] Whelley P. L. and Greeley R. (2006), *JGR*, 111, 1-5. [6] Hendriks, C. L. L. *IEEE Trans. Image Proc.*, 19, 1587-1595.